Oxidation of N-doped multiwalled carbon nanotubes and formation of discontinuous spiraled carbon nanoribbons

Aman Preet Kaur,[a,b] Mark S. Meier,*[a,b] Rodney Andrews,[b,c] and Dali Qian[b]

[a]*Department of Chemistry, University of Kentucky, Lexington, KY 40506-0055*
[b]*Center for Applied Energy Research, University of Kentucky, Lexington, KY 40511-8479*
[c]*Department of Chemical and Materials Engineering, University of Kentucky, Lexington, KY 40506-0046*
Email: meier@uky.edu

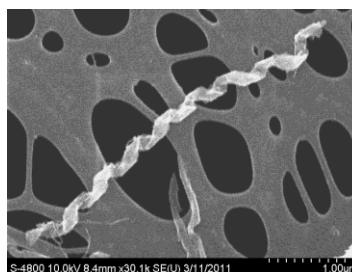**Dedicated to Professor Gordon W. Gribble on the occasion of his retirement from Dartmouth College**

Abstract

The effects of five commonly used wet chemical oxidations were studied for the extent of oxidation of graphitized nitrogen-doped multiwalled carbon nanotubes (N-MWCNTs). $KMnO_4$/ H_2SO_4 was the most potent oxidant, as it produced the highest fraction of oxygen-containing functional groups. Electron microscopy studies showed that the treatment of annealed N-MWCNTs (G-N-MWCNTs) with H_2SO_4/HNO_3 and H_2SO_4/$KMnO_4$ mixtures leads to interesting spiraled ribbon textures. A structural model, involving the stacking of coiled subunits to form a discontinuous carbon nanoribbon rather than a continuous ribbon is proposed to explain the range of textures that result from oxidation as well as from reduction.

Keywords: N-MWNTs, stacked-cup carbon nanotubes, carbon ribbons

Introduction

Since their discovery,[1-3] carbon nanotubes (CNTs) have presented unparalleled potential because of their combination of extraordinary mechanical, electrical, and thermal properties.[4-7] With appropriate surface modifications of CNTs, these properties can be harnessed in a variety of applications.[8-11] Thus far, covalent and non-covalent functionalizations[12,13] have been widely investigated approaches to modify these materials. One common method for modification of CNTs is "wet" chemical oxidation[14] that provides the dual advantages of purification of the raw material[14] and as well as improving the dispersibility of CNTs.[15]

Chemical literature on CNTs includes several reports on methods[16,17] and effects[18-20] for oxidation of single-walled carbon nanotubes (SWCNTs) and multi-walled carbon nanotubes (MWCNTs) under both acidic and basic conditions. Commonly used methods include treating CNTs with HNO_3,[21,22] mixtures of H_2O_2/H_2SO_4 (piranha solution),[16] H_2SO_4/HNO_3,[20,23] and NH_4OH/H_2O_2,[17] $KMnO_4$,[24,25] O_3[26] as well as others. Treatment of SWCNTs with hot HNO_3 helps in efficient removal of metal impurities and graphitic platelets.[21] Bower et al.[27] have reported the intercalation of nitric acid molecules into SWCNT bundles, and prolonged exposure leads to exfoliation and to etching of carbon. High temperature annealing following nitric acid-treatment has also been used to remove amorphous carbon.[28] Shortening of MWCNTs and formation of amorphous carbon were observed with prolonged exposure to concentrated HNO_3.[22]

Specific conditions for oxidation of CNTs with piranha solution can bring about controlled cleavage of CNTs.[16,29] At higher temperatures, piranha solution attacks defect and damage sites, creating vacancies in the sidewalls. Increasing the exposure time results in shorter nanotubes from further oxidation of these vacancies. Selective etching of smaller diameter nanotubes and significant sidewall damage are other results of this process.[16] At room temperature, piranha solution is not as efficient and results in less etching and less sidewall damage.

Treatment of MWCNTs with a mixture of H_2SO_4 and HNO_3 for 6 hours or more purifies and oxidizes the nanotubes, but also causes opening of closed ends.[30] The highly curved surfaces at the end of nanotubes are fullerene-like, and it is easy to understand why these sites would be susceptible to oxidation. Cho *et al.* reported radial followed by longitudinal unzipping of MWCNTs using a chemical method containing H_2SO_4 and HNO_3.[31] Lengthwise opening of MWCNTs along their axis was observed by Tour et al.[24] with a mixture of H_2SO_4 and $KMnO_4$.

The effects of oxidation under different conditions have been evaluated with a variety of analytical methods including microscopy (SEM, TEM, AFM), thermal methods (TGA, DTA, TPD), X-ray photoelectron spectroscopy, Raman spectroscopy, energy dispersive X-ray spectroscopy, infrared spectroscopy, NMR and EELS.[32,33]

Despite the availability of variety of oxidizing approaches for the modification of SWCNTs and MWCNTs, the mechanism of action of these reagents on different nanotube sites is rarely discussed.[18,24] Zhang et al.[18] proposed that the original or newly created defects on CNTs play a crucial role during the oxidation process. With this idea they explored oxidation reactions under different conditions and predicted intermediates and final products based upon their observation and analysis.

In nitrogen-containing multiwalled carbon nanotubes (N-MWCNTs) (Figure 1) the central core is periodically bridged, giving a texture similar to a set of stacked cups.[34,35] In this arrangement, the axes of graphene planes are not parallel to the tube axis, so each graphene sheet must terminate at the surface.
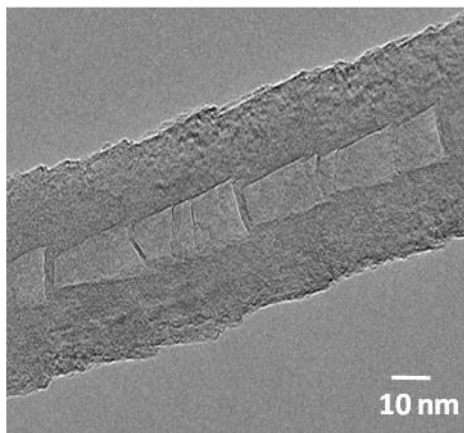
Figure 1. TEM image of thermally-annealed pyridine-derived N-MWCNTs (G-N-MWCNTs).

We anticipated that the large number of exposed edges would make these materials more reactive than classical cylindrical MWCNTs in which the outer surface is a gently curved graphene plane rather than a set of exposed edges. In this study, we present the results of five different chemical oxidation methods on thermally annealed (graphitized) N-MWCNTs (G-N-MWNTs). The resulting oxidized N-MWCNTs were characterized using thermogravimetric analysis and electron microscopy.

Result and Discussion

N-MWCNTs were prepared at the UK Center for Applied Energy Research from a pyridine feedstock containing dissolved ferrocene as catalyst, at a temperature of 800 °C in a 4 inch diameter quartz tube reactor using N_2 as the carrier gas. [36] Annealing/graphitization of this material was carried out in a graphite crucible at 2800 °C in a helium atmosphere. This process removes the nitrogen and the residual catalyst, and anneals the material[37] by removing structural defects, making the graphene sheets as perfect as possible, yet not necessarily following the Bernel stacking. We refer to the resulting tubes as G-N-MWCNTs (Figure 1).[35] The material was subjected to five different sets of oxidizing conditions: 1) refluxing HNO_3; 2) H_2SO_4/H_2O_2; 3) $FeSO_4/H_2O_2$; 4) H_2SO_4/HNO_3; and 5) $KMnO_4/ H_2SO_4$.

Oxidation with concentrated HNO_3

Thermal gravimetric analysis (TGA) was used to determine the thermal stability of each material in air, which provides an indication of the extent of damage (if any) to the graphene sheets. G-N-MWCNTs (black curve in Figure 2) start to oxidize at ~ 660 °C, reflecting the low defect density and more perfect structure that results from the high-temperature annealing (Figure S1).[38] The low temperature thermal degradation and the shift of the onset of the oxidative decomposition to lower temperature in G-N-MWCNTs that were subjected to sonication (30 min) followed by refluxing in conc. HNO_3 for 6 hours (blue), 12 hours (green) and 24 hours (red), compared to G-N-MWCNTs suggests introduction of functional groups and defects upon acid treatment.
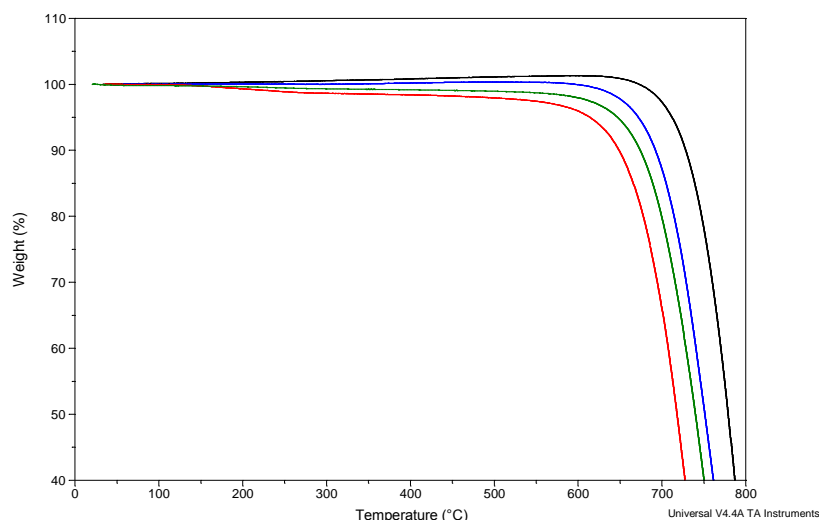
Figure 2. Thermogravimetic analysis (TGA) comparing G-N-MWCNTs (black) with products of conc. HNO_3 oxidation: 6 hours (blue), 12 hours (green) and 24 hours (red).

As reported in TGA experiments conducted on oxidized MWCNTs, the thermal oxidative degradation is a multistage process[17] and it is likely that oxidative degradation of G-N-MWCNTs (Figure 2) is similar. The low temperature weight loss can be attributed to evaporation of physisorbed water, decarboxylation and elimination of water from hydroxyl functionalities. The observed degradation at higher temperatures is a result of thermal oxidation of remaining disordered carbon. The decrease in the temperature of the onset of the oxidative decomposition upon increasing reflux time periods is evidence of increasing G-N-MWCNT structural damage as suggested by SEM (below).

SEM and STEM were used to study the morphological changes in G-N-MWCNTs texture after each oxidation treatment. Treatment of MWCNTs with conc. HNO_3 results in shortening, fragmentation[22], and degradation of CNTs to carbonaceous materials.[22,27] However, with G-N-MWCNTs no drastic change in length or in the fragmentation of CNT was observed (Figure 3).

SEM images (Figure 3a) of G-N-MWCNTs that had been refluxed in conc. HNO_3 for 6 hours showed limited damage on tubes, although initiation of exfoliation and etching of the surface (Figure S2) are evident. While only partial exfoliation was seen after 12 hours, greater exfoliation resulting in formation of carbonaceous material was observed after 24 hours.
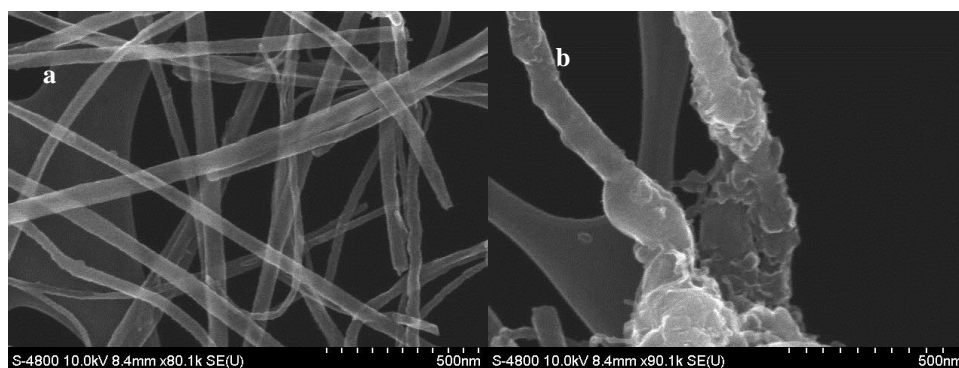

Figure 3. SEM images of G-N-MWCNTs treated with conc. HNO_3 after: a) 6 hours; and b) 24 hours reaction time.

Oxidation with H_2SO_4/H_2O_2 (piranha oxidation)

Piranha solution (H_2SO_4/H_2O_2) appears to be significantly milder than HNO_3 in its effects on G-N-MWCNTs. Stirring a suspension of G-N-MWCNTs with piranha solution at room temperature did not result in significant changes as reflected by TGA (Figure 4) until roughly 24 hours (red) of treatment.
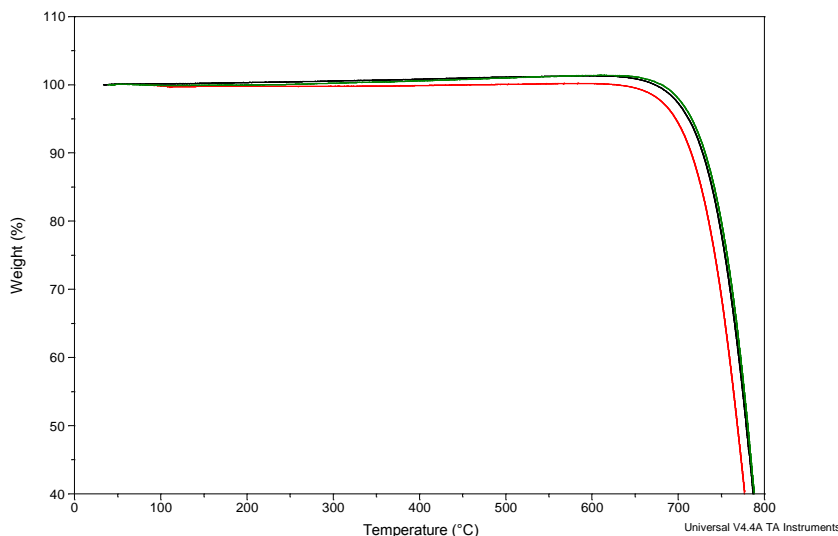

Figure 4. TGA comparing G-N-MWCNTs (black) with products of oxidation with piranha solution after: 12 hours (green) and 24 hours (red) of oxidation.

SEM results (Figure 5) supported the observations from TGA and indicated very little damage of the tubes from oxidation with piranha solution. The tubes appeared unaffected after 12 hours (Figure 5a) of piranha treatment and most of the tubes were unaffected even after 24 hours (Figure 5b). Only few of the tubes appeared to have significantly damaged side-walls (Figure S3f).
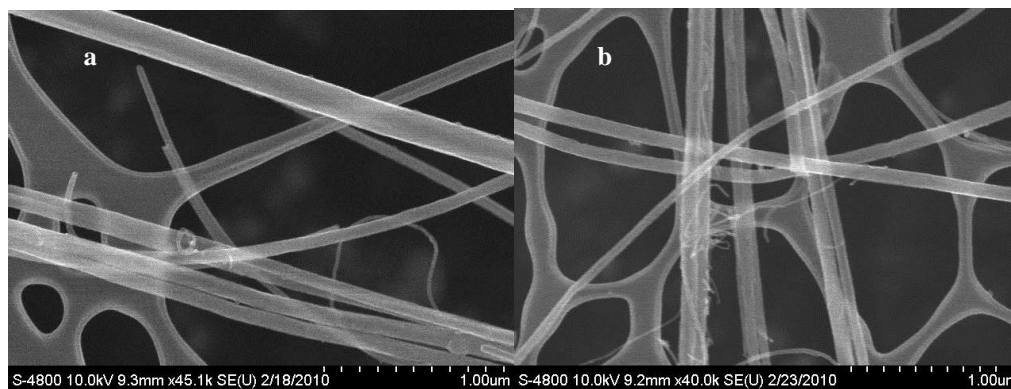

Figure 5. SEM images of G-N-MWCNTs treated with piranha solution after: a) 12 hours reaction time; and b) 24 hours reaction time.

Wang et al. have shown that a mixture of H_2O_2 and HCl can significantly increase purity of as-produced nanotube material.[39] They proposed that the presence of Fe particles in the as-produced material acts as a catalyst for Fenton chemistry, producing hydroxyl radicals which are a more powerful oxidant than H_2O_2. The absence of Fe catalyst in our materials means that there is no iron source during piranha oxidation so no

Fenton chemistry would occur, and this may be responsible for insignificant effect of piranha oxidation. This led us to explore the effects of Fenton oxidation.

Oxidation with FeSO$_4$/H$_2$O$_2$ (Fenton Oxidation)

TGA (Figure 6) of the material obtained by treatment of G-N-MWCNTs with Fenton's reagent at room temperature for 24 hours had two striking features. Comparing the thermal stability of Fenton oxidized material to that of G-N-MWCNTs, we can see that there is 150 °C difference between the T_o of the two materials. There is also a 10% increase in residue, a red solid that is likely Fe$_2$O$_3$. There were no noticeable dark spots on individual tubes (Figure 7) when the product was imaged using STEM. EDX (Figure S4) on G-N-MWCNTs treated with Fenton's reagent showed no peaks from Fe. Instead, we observed a few dark big pieces (Figure S5) isolated from tubes under STEM and EDX on these showed Fe. So, we suspect these to be residual iron that showed as a residue in TGA. The product was treated with 48 wt% HBr in order to effectively remove iron. The difference was clearly seen in TGA (Figure 6), with red curve representing the oxidative thermal degradation of the HBr treated material following Fenton oxidation. Also, the difference in T_o was reduced from 150 °C to 70 °C, implying that residual iron having a catalytic role in oxidative thermal degradation.

Comparing piranha oxidation (Figure 4-red curve) with Fenton oxidation (Figure 6b-green curve), it can be concluded that Fenton oxidation causes more damage than does piranha solution, as the onset of oxidation is shifted to a lower temperature. STEM images (Figure 7) also suggest more side-wall damage in case of Fenton oxidation, supporting the TGA results. Based on these observations, the piranha oxidation in as-produced, iron-containing MWCNTs is likely a Fenton oxidation, resulting from oxidation of the iron catalyst particle to form Fe(II) ions that lead to Fenton chemistry.
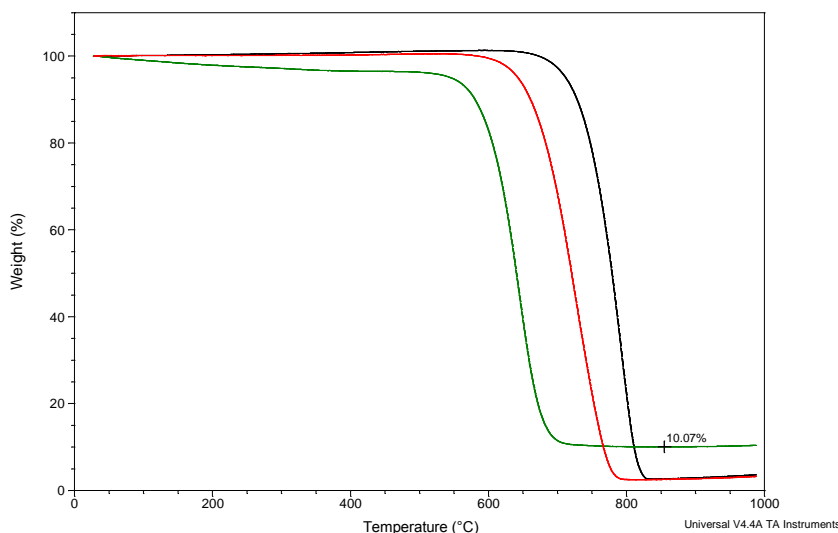

Figure 6. TGA comparing G-N-MWCNTs (black) with product of Fenton oxidation (green), and HBr treatment to remove iron (red).
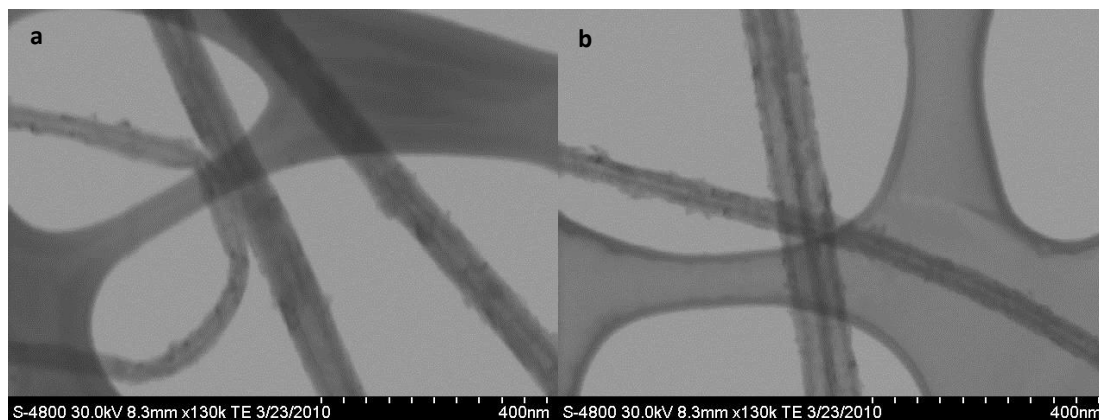
Figure 7. STEM images of G-N-MWCNTs treated with Fenton's reagent.

Oxidation with H_2SO_4/HNO_3

Acid oxidation treatment of G-N-MWCNTs, with a mixture of H_2SO_4 and HNO_3 (3:1) with sonication at room temperature (Figure 8) shifted the onset of oxidation to a lower temperature, both at 12 hours (green) and 24 hours (red) compared to that observed under treatments 1, 2 and 3 discussed above. This shift may likely be the result of increased damage to the tubes, consistent with what was found by SEM analysis.
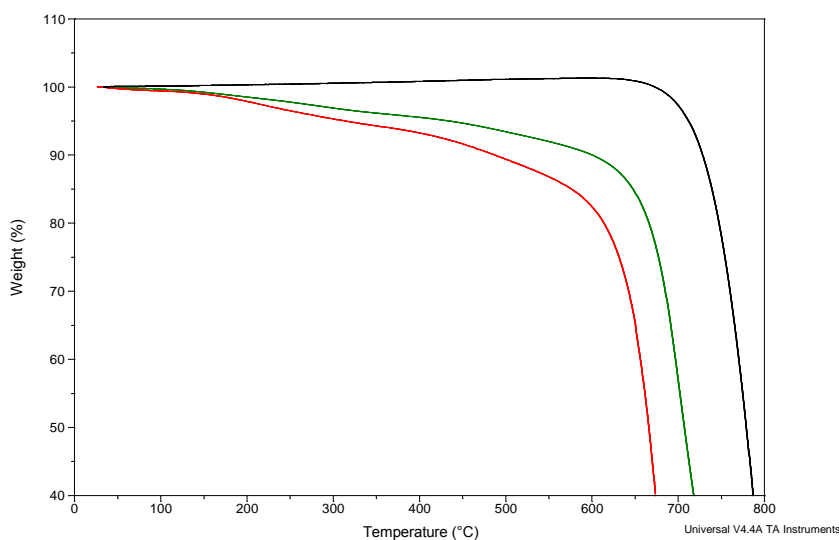

Figure 8. Thermal gravimetric analyses comparing G-N-MWCNTs (black) with products of oxidation with a mixture of H_2SO_4 and HNO_3 (3:1): 12 hours (green) and 24 hours (red).

Sonicating G-N-MWCNTs in a mixture of H_2SO_4 and HNO_3 (3:1) for 12 hours resulted in the formation of spiraled ribbons (Figure 9). Carbon ribbon structures have been observed by others after oxidation of stacked-cup nanotubes.[40] We have previously reported the phenomenon of longitudinal cutting in N-MWCNTs[34,35] under dissolving metal reduction conditions (Li metal in liquid ammonia or ethylenediamine). The most common morphology of fractures observed after oxidation in this mixture was spiraled ribbons.
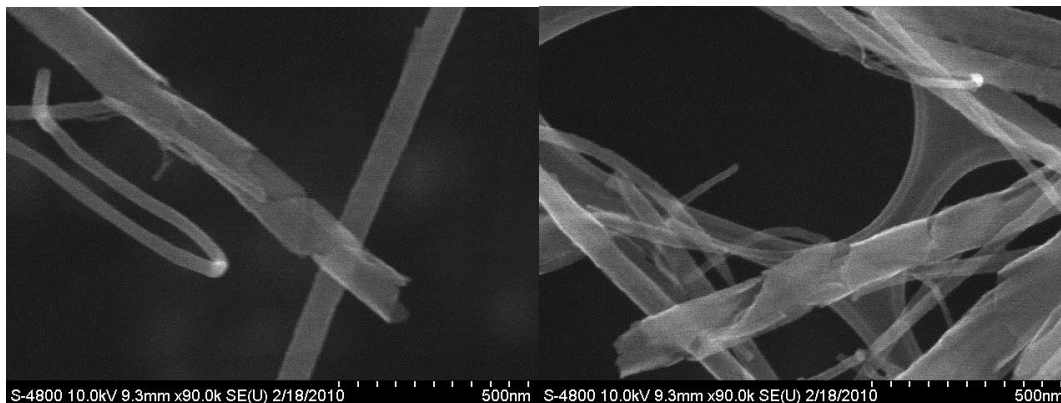

Figure 9. SEM images of G-N-MWCNTs treated with H_2SO_4/HNO_3 (sonication for 12h).

In order to determine if the oxidizing mixture or the sonication were responsible for the fractures, the tubes were stirred for 12 hours in the same mixture. To our surprise, the spiraled ribbons were still formed (Figure S6).　When the time period of sonication was increased from 12 to 24 hours, more damaged tubes were seen. The tubes became shorter as reflected by SEM (Figure 10). The formation of spiraled ribbons was also confirmed by running SEM and STEM simultaneously (Figure S7).
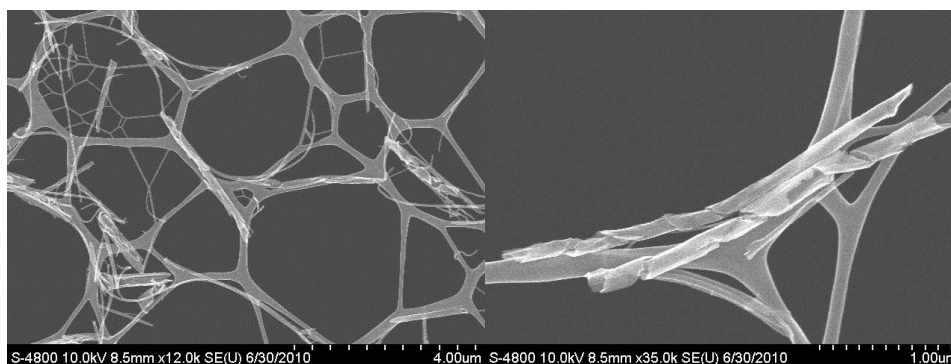

Figure 10. SEM images of G-N-MWCNTs treated with H_2SO_4/HNO_3 (sonication for 24h).

It has already been observed that sonication of SWCNTs in H_2SO_4/HNO_3 (3:1) mixture produces tubes of shorter lengths, as microscopic domains of high temperature produced by the collapse of cavitation attack the surface of the tubes, leaving an open hole in the tube side.[14] Subsequent attack by the acid mixture at this newly created defect cuts the tube cleanly.

We further evaluated the structure of the G-N-MWCNTs before and after treatment using Raman spectroscopy. It was clear (Figure 11a) from the ratio of the integrated intensities of the D (1353 cm^{-1}) band to G (1576 cm^{-1}) band that G-N-MWCNTs have very few defects (I_D/I_G ~ 0.13) and upon oxidation (Figure 11b) with H_2SO_4/HNO_3 mixture the G band broadens a little with significantly increased intensity of the D band. It has been reported that oxygen-containing functionalities such as carbonyls, carboxyls and hydroxyls[41] exist at the edges and the surface,[42] thereby disrupting the π-conjugated network, which results in broadened G band and increased intensity of D band.[24]
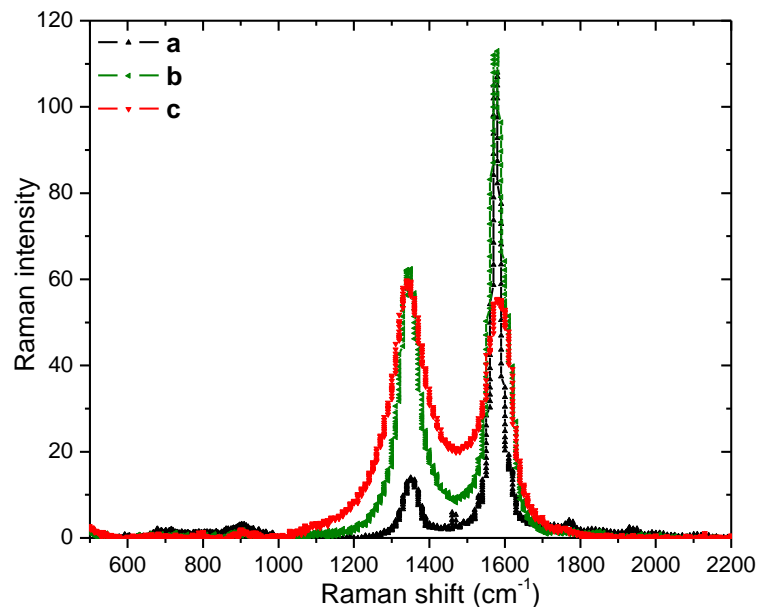
Figure 11. The Raman spectra of: a) G-N-MWCNTs; b) G-N-MWCNTs treated with H_2SO_4/HNO_3 (sonication for 24h) and c) G-N-MWCNTs treated with $KMnO_4/H_2SO_4$.

We used XPS to determine the composition of oxidized compared to the starting G-N-MWCNTs which corresponds to the data shown in Figure 12. XPS spectroscopy also confirmed that the atomic concentration of oxygen increased from 3 to 12%.

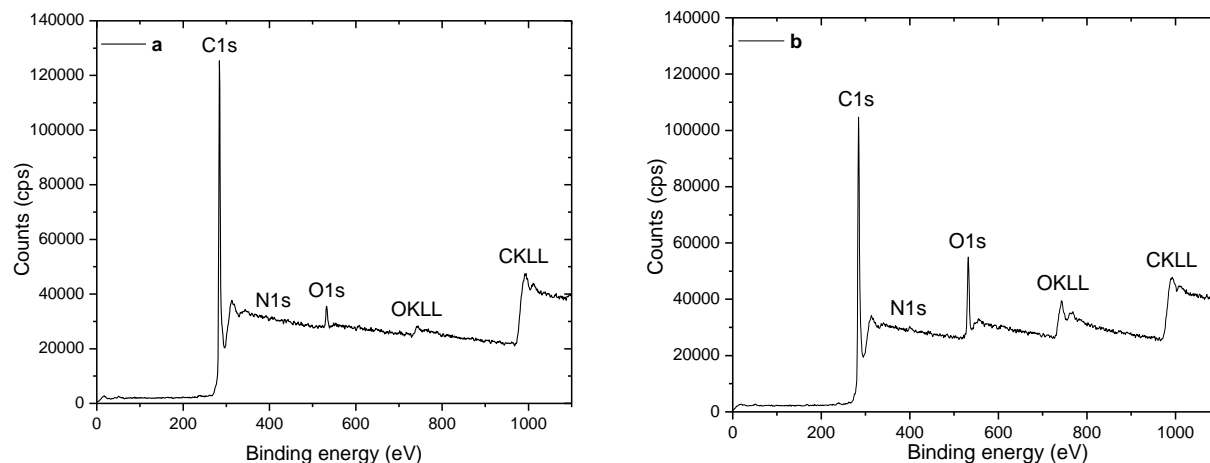**Figure 12.** The XPS spectra of: a) G-N-MWCNTs and b) G-N-MWCNTs treated with H_2SO_4/HNO_3 (sonication for 24h).

Oxidation with $KMnO_4/H_2SO_4$

Among all the acid oxidative treatments on G-N-MWCNTs, $KMnO_4$ oxidation conditions remain the harshest. TGA (Figure 13, curve red) showed considerable low temperature weight loss (~55%) attributed to evaporation

of physisorbed water, decarboxylation, decarbonylation and elimination of hydroxyl functionalities and also a maximum shift in the onset temperature of oxidation of remaining disordered carbon.
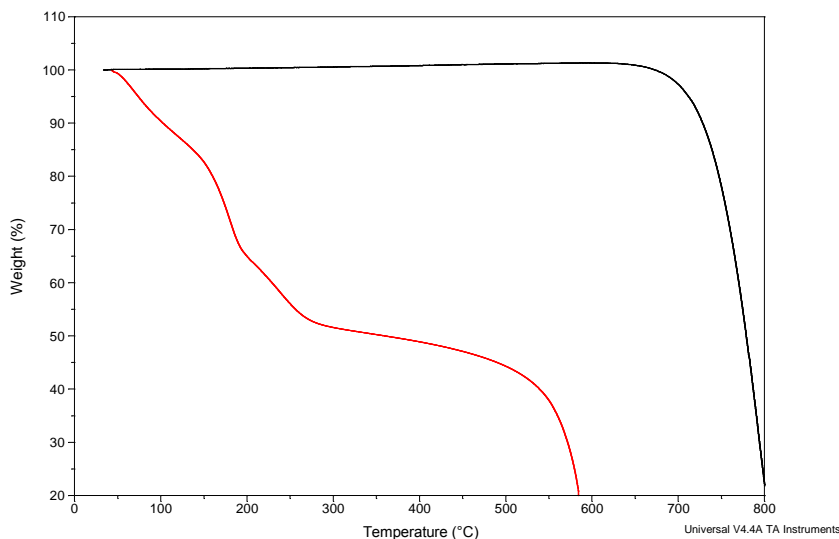

Figure 13. Thermal gravimetric analysis comparing G-N-MWCNTs (black) with $KMnO_4/H_2SO_4$ oxidized product (red).

We also performed XRD analysis (Figure 14) to further investigate this high degree of oxidation as was observed from TGA. G-N-MWCNTs have 2ϑ values of ~26.18˚, corresponding to a d-spacing of 3.4 Å. $KMnO_4$ oxidized G-N-MWCNTs show a predominant peak at 2ϑ = 10.7˚, corresponding to a d spacing of 8.3 Å, with minimal signal contributed by G-N-MWCNTs (2ϑ = 26˚). The spectrum is similar to that of graphite oxide (GO) prepared by Hummers method.[41]
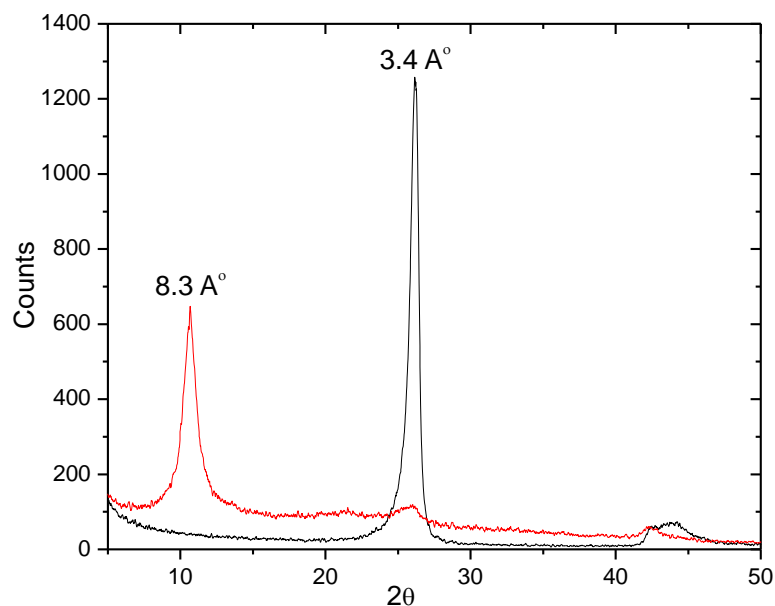

Figure 14. XRD analysis comparing G-N-MWCNTs (black) and $KMnO_4/H_2SO_4$ oxidized G-N-MWCNTs (red).

Raman spectroscopy also supported the increased level of disorder with the $KMnO_4$ oxidized material having $I_D/I_G \sim 1.1$ (Figure 11c) compared to $I_D/I_G \sim 0.13$ (Figure 11a) for G-N-MWCNTs. This behavior is similar to that observed for GO with a broadened G peak (1577 cm^{-1}) after oxidation along with the dramatic appearance of the D band at 1342 cm^{-1}.

Microscopy (Figure 15) revealed that $KMnO_4$ oxidation on G-N-MWCNTs also produced these unusual spiraled ribbon textures. Shortening of tubes lengthwise was not observed from the SEM and TEM (Figure S8) images, unlike what is observed after oxidation with H_2SO_4/HNO_3. Also, the morphology of these spiraled ribbons was quite different from the ones we had seen before with reducing[35] as well as oxidizing (H_2SO_4/HNO_3) conditions. Here, the ribbon texture is more distinct, with the distance between the turns of the helix being 100-150 nm.

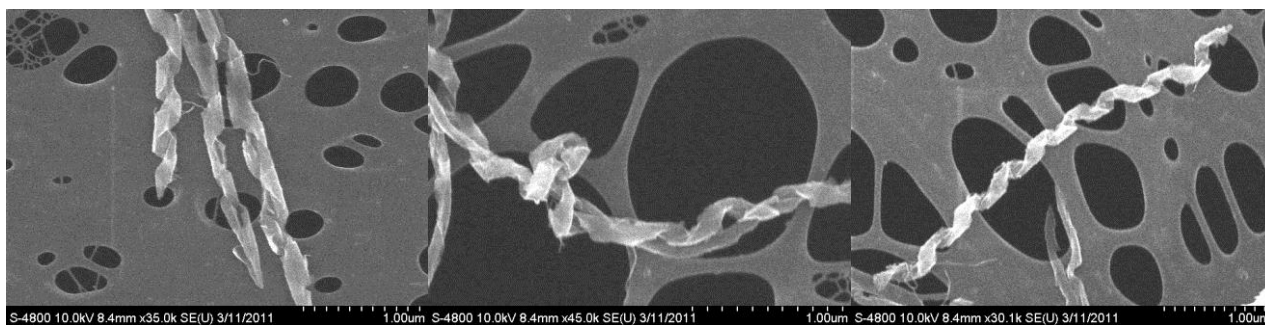**Figure 15.** SEM images of $KMnO_4/H_2SO_4$ oxidized G-N-MWCNTs.

XPS and EELS analysis were further used to quantify the atomic concentration of oxygen. From the work of Tour *et al.*, in the XPS carbon 1*s* spectra (Figure 16b) of the $KMnO_4$ oxidized G-N-MWCNTs, the signals at 286 eV and 287 eV correspond to C–O and C=O, respectively and the shoulder at 289 eV is assigned to carboxyl groups.[24] In addition, the atomic concentration of oxygen increased from 3% to 20% as determined by XPS.

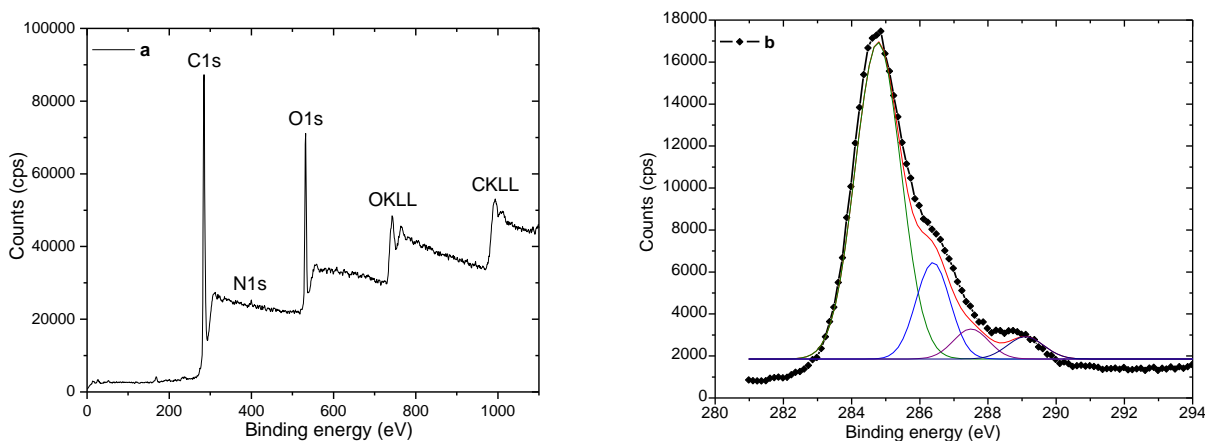**Figure 16.** a) XPS and b) deconvoluted C 1*s* spectra of $KMnO_4/H_2SO_4$ oxidized G-N-MWCNTs.

EELS analyzed from individual oxidized tubes (STEM mode) exhibits the O-K edge at ~535 eV and the C-K edge at ~290 eV. It is clear (Table 1) that oxygen-containing functional groups are distributed on the surface as

well as the edges of the tubes. It can be seen that the average oxygen content is in accordance with that reported by XPS analysis, as a large fraction of oxygen atoms are located at or near to the surface.

Table 1. Quantitative atomic percent content of C and O measured by EELS at three different spots

Location	C (at. %)	O at. %
Spot 1	79	21
Spot 2	74	26
Spot 3	81	19

The surface area of these carbon ribbons was determined by nitrogen physisorption at 77K performed to calculate the BET surface area. These results showed that upon oxidation of G-N-MWCNTs with a mixture of H_2SO_4/HNO_3 (sonication for 24 hours), the surface area increased from 34 m^2/g to 63 m^2/g which was lower than what we have observed for samples treated under reducing conditions.[34,35] Upon $KMnO_4$ oxidation of G-N-MWCNTs, the surface area increased to 240 m^2/g, with a total pore volume of 0.54 cm^3/g and the resulting material was highly mesoporous (~ 75%) which can easily be seen from the nitrogen adsorption isotherm (Figure 17a) and corresponding plot of incremental surface area vs. pore width (Figure 17b).
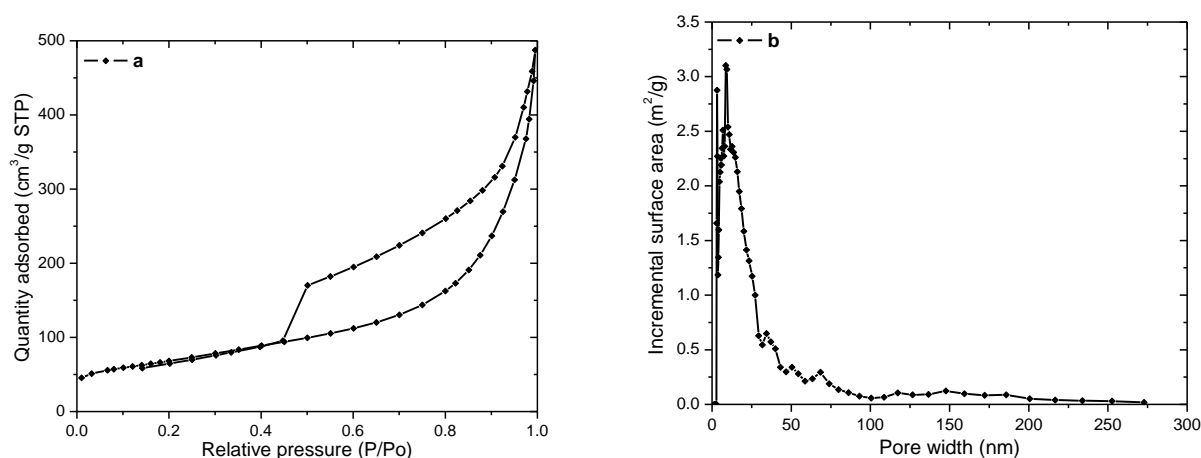

Figure 17. a) Adsorption isotherm and b) plot of incremental surface area vs. pore width in $KMnO_4/H_2SO_4$ oxidized G-N-MWCNTs.

The material exhibits a type IV isotherm with a steep condensation step between 0.50 and 0.45 P/ P_o, indicating the formation of new mesopores,[43] while G-N-MWCNTs showed virtually no hysteresis in the nitrogen desorption loop. The pronounced hysteresis loop seen in the Type IV nitrogen adsorption isotherm exhibited by this material is indicative of capillary condensation in mesopores, and likely reflects the addition of mesoporosity due to opening of the cores rather than addition of external surface roughness which would increase area but would result in a more conventional adsorption behavior without capillary effects. It should also be noted that the isotherm (Figure 17a) lacks a high-pressure plateau, usually indicative of a narrow pore size distribution with pore sizes tending toward the smaller end of the mesopore regime, as exhibited here (Figure 17b).

The observation of longitudinal cutting of G-N-MWCNTs under widely differing conditions (reducing conditions with Li/NH$_3$[34,35] and oxidizing conditions with KMnO$_4$/H$_2$SO$_4$ and with HNO$_3$/H$_2$SO$_4$) suggests that this material has a morphology that makes it predisposed to react in the manner described above. It also suggests that the process is largely physical rather than chemical, and accordingly we believe that intercalation is the driving force behind the observed changes from a "stacked cup" appearance to the spiraled ribbons shown above, as well as to other morphologies reported earlier.[34,35]

Lithium is known to form intercalation compounds with carbon materials like graphite[44] and MWCNTs.[45] Sulfuric acid is also known to intercalate into MWCNTs.[31] Cho *et al.*[31] observed radial followed by longitudinal unzipping of MWCNTs in mixtures of HNO$_3$ and H$_2$SO$_4$ with high mixing ratio of H$_2$SO$_4$ (1:3 and 1:4). We have observed longitudinal opening of our material in a mixture of HNO$_3$/H$_2$SO$_4$ (1:3) but not upon refluxing in HNO$_3$. So, under oxidizing conditions, intercalation of H$_2$SO$_4$ seems to be a key requirement for opening the material, resulting in either separation of graphene layers or facilitating cleavage of C-C bonds. Sulfuric acid, but not strong oxidation is likely required for opening these tubes. In the piranha oxidations reported in the current work, H$_2$SO$_4$ is present but at such a low concentration that appears to be ineffective in causing any change in the appearance of G-N-MWCNTs.

We believe that oxidation/intercalation pushes apart segments of the N-MWCNT structure and exposes the underlying morphology, and that the underlying morphology is most likely not a set of stacked cups. Other models are proposed for explaining the texture of members of the "stacked cup" or herringbone family of filamentous carbons. These involve a discontinuous arrangement formed by stack of truncated graphitic cones[46-49] or a continuous texture formed by a helical graphene ribbon wrapped into a conical spiral.[48-51] It has been found that stacked cup texture is distinct from herringbone arrangement although they can look similar in TEM images.[52]

Monthioux *et al.*[48-51] found dramatic variations in type, diameter, inner texture and structure of filamentous carbon materials as a function of the catalyst composition and preparation method. They have estimated the relative proportions of various nanofilament types (platelet nanofiber to herringbone nanofiber to herringbone-bamboo nanotubes) depending on the angle (α) between graphene layers with respect to the nanofilament axis. Materials grown with graphene angles (α) that range from 30° to 180° take on herringbone nanofiber to herringbone-bamboo nanotube textures.
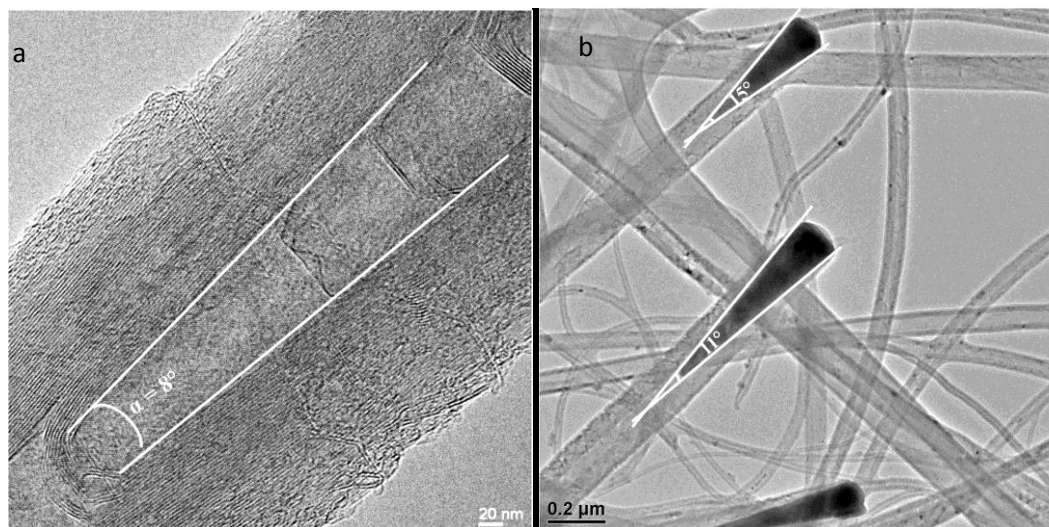

Figure 18. HRTEM images showing a) the α angle in G-N-MWCNTs; and b) the conical catalyst particles in N-MWCNTs before annealing.

In our material, the graphene layers are arranged with very narrow angles (7-12°) relative to the nanotube axis (Figure 18a), compared to the >30˚ angles studied previously. We observe catalyst particles (Figure 18b) that are sharp cones with angles ranging from 8˚ to 15°, significantly more pointed than the elongated conical catalyst particles (20˚ - 60°) observed by Monthioux *et al..* [48-51]

In an effort to understand more about the texture we attempted to pull these spiraled ribbons lengthwise by stretching a polymer composite. Composites containing these ribbons in polystyrene (PS), polyethylene (PE) and poly(methyl methacrylate) (PMMA) were formed by casting a suspension of the spiraled ribbons in a solution of polymer dissolved in THF. Stretching and breaking the composite did not expose ribbons, but it was observed that focusing the SEM electron beam on a PMMA-CNT composite initiates cracks in the surface of the composite and exposes examples of these ribbons. The SEM image shown in Figure 19a shows a structure that is composed of a stack of coiled subunits, not a continuous coiled ribbon. Even in situations where the spiraled ribbons are found exposed at the surface of the composite, they do not appear as continuous coiled ribbons but instead as a set of coiled subunits (Figure 19b). We believe that the subunits visible in Figure 19 are composed of multiple graphene layers rather than a single sheet of graphene.
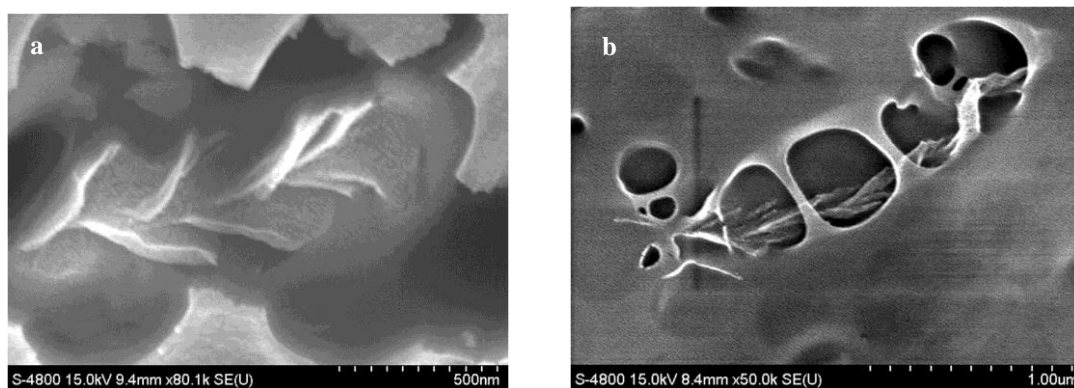

Figure 19. SEM image of KMnO$_4$/H$_2$SO$_4$ oxidized G-N-MWCNTs within a PMMA composite. a) exposed within a void in the composite; b) exposed on the unmodified surface of the composite.

We have observed similar spiral textures, as well as linear channels, formed under conditions of dissolving metal reduction followed by alkylation of G-N-MWCNTs.[34,35] Formation of spiraled channels (a carbon "ribbon") or linear channels, starting from the same material and under completely different conditions, can be rationalized as resulting from movement of the subunits that make up the structures in Figure 19 above. Oxidation/intercalation (or reduction/intercalation) opens up the structure and permits the subunits to move relative to each other. If they do not rotate, the aligned edges of the subunits appear as a linear channel. If the edges of the subunits slip relative to each other, a curving channel is formed, and with slight rotation of subunit, a spiral ribbon forms, albeit a ribbon formed from the multiple subunits rather than from one continuous band of graphene.

When treated with a dilute polymer solution, the spiraled ribbons have a thin polymer coating on their surface. In some STEM images (Figure 20), this highlighted their surface texture and it is possible to see the edges of the individual subunits that together create the impression of a continuous coiled ribbon.
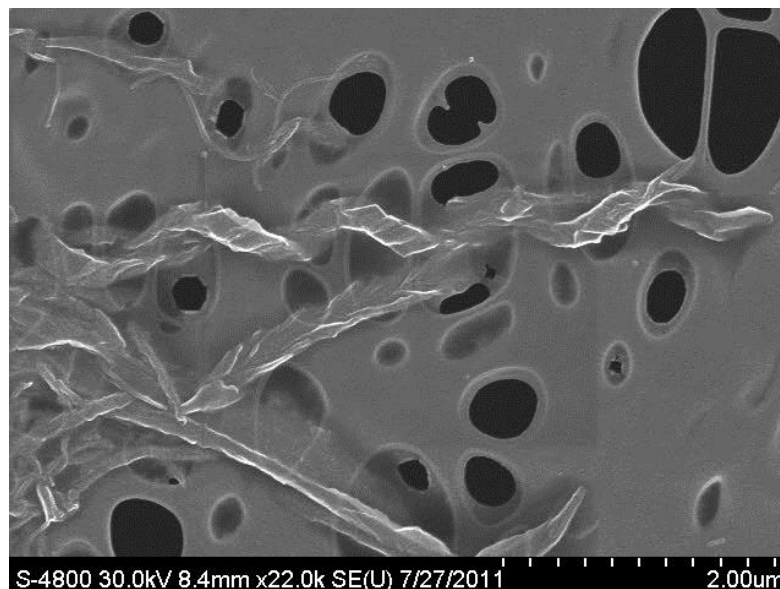
Figure 20. STEM-SEM image of PMMA-KMnO$_4$/H$_2$SO$_4$ oxidized G-N-MWCNTs composite.

Conclusions

We have investigated the effect of a range of different oxidation techniques on thermally annealed N-MWCNTs and have found that H$_2$SO$_4$/H$_2$O$_2$ produces little change in the material, but that KMnO$_4$/H$_2$SO$_4$ produces interesting discontinuous spiraled ribbon textures. We believe that this result indicates that many of the N-MWCNTs we produced by CVD synthesis from pyridine/ferrocene in our reactor do not have either a true stacked-cup texture or a continuous carbon ribbon texture, but are instead a stack of small coiled subunits. We believe that oxidation/intercalation pushes apart the stacks, revealing and enabling the subunits to move relative to each other, resulting in the appearance of spiraled carbon nanoribbons. Stacked cup nanotubes and their oxidized forms are highly mesoporous and may have interesting applications in power storage devices,[53,54] diodes,[55] and biosensors.[56]

Experimental Section

Treatment 1 (conc. HNO$_3$).[17,22] A suspension of 0.25 g of G-N-MWCNTs in HNO$_3$ (70 wt%, 50 mL) was subjected to bath sonication for 30 min. The flask was then equipped with a condenser and a magnetic stir bar. The dispersion was stirred and heated at reflux for periods of 6, 12 and 24 h. After that, the resulting dispersion was diluted in H$_2$O, filtered and washed with H$_2$O to neutral pH and then with EtOH. The resulting solid was dried in vacuum for overnight.

Treatment 2 (piranha).[17] A suspension of 0.25 g of the G-N-MWCNTs in 50 mL of a mixture of H$_2$SO$_4$ (96 wt%) and H$_2$O$_2$ (30 wt%) in ratio 70:30 in a 100 mL round bottom flask equipped with a condenser and the mixture was stirred at rt for periods of 12 and 24 h. After that, the resulting dispersion was diluted in H$_2$O, filtered and washed with H$_2$O to neutral pH and then with EtOH. The resulting solid was dried in vacuum for overnight.

Treatment 3 (Fenton). G-N-MWCNTs (0.25 g) was added to 75 mL of H$_2$O in a 250 mL round bottom flask. To the stirred solution were added FeSO$_4$.7H$_2$O (125 mg) and then H$_2$O$_2$ (30%, 25 mL). The solution was allowed to

stir for 24 h, filtered, washed with H_2O and EtOH and dried in vacuum overnight. The residual iron was removed by stirring the product with HBr (48 wt%, 20 mL) for 6 h.

Treatment 4 (conc. H_2SO_4:HNO_3).[23] To G-N-MWCNTs (0.25 g) was added 50 mL of a 3:1 mixture of H_2SO_4 (96 wt%) and HNO_3 (70 wt%). The mixture was subjected to bath sonication at rt for periods of either 12 or 24 h. After that, the resulting dispersion was diluted in H_2O, filtered and washed with H_2O to neutral pH and then washed with EtOH. The resulting solid was dried in vacuum overnight.

Treatment 5 ($KMnO_4$:H_2SO_4).[24] G-N-MWCNTs (0.15 g) was suspended in conc. H_2SO_4 (150 mL) for 24 h, then $KMnO_4$ (750 mg, 4.75 mmol) was added. After stirring for 1 h at rt, the mixture was heated at 55 °C for 30 min. The temperature was further increased to 65 °C for 15 min and finally to 70 °C. When the temperature stabilized at 70 °C, the reaction mixture was removed from heating and allowed to cool to rt. The mixture was poured into ice H_2O (400 mL) containing H_2O_2 (30%, 5 mL). The solid material was filtered off under vacuum through a PTFE membrane. Following stirring of solid material in H_2O (150 mL) for 30 min, it was subjected to bath-sonication for another 15 min. Addition of 20 vol% conc. HCl (30 mL) flocculated the material that was again filtered through a PTFE membrane. The solid material obtained was stirred in EtOH (150 mL) for 30 min and then bath-sonicated for 15 min. Flocculation occurred on addition of Et_2O (100 vol%, 150 mL) and the product was collected by filtration through a PTFE membrane. Washing with Et_2O (2 x 50 mL) and drying *in vacuo* afforded oxidized nanotubes (270 mg).

Sample characterization. After the oxidation experiments, the samples were characterized by thermogravimetric analysis (TGA, TA 2950 with a standard heating rate of 10 °C/min from ambient temperature to 1000 °C under air), scanning electron microscopy (Hitachi S-4800 FE-SEM), transmission electron microscopy (JEOL 2010F at an acceleration electron voltage of 200 kV) and N_2 physisorption at 77 K (Micromeritics ASAP 2020 V3.00H) after pre-outgassing at 300 °C for 12 h. Surface areas and pore size distributions were calculated from the adsorption isotherms using the BET model. X-ray photoelectron spectra (XPS) of samples were recorded using a Physical Electronics PHI 5400 spectrometer with a magnesium X-ray source. X-ray powder diffraction (XRD) analysis was performed using a Bruker AXS (model D8 DISCOVER) at Kentucky Geological Survey facility with Cu Kα lamp. Raman spectroscopy was recorded with Thermo Scientific DXR Smart Raman (532 nm laser excitation).

Acknowledgements

Supplementary Material

The supplementary materials, Figures S1-S8 and Table S1, are available in the online version of the text.

References

1.　Monthioux, M.; Kuznetsov, V. L. *Carbon* **2006**, *44*, 1621.
　　https://doi.org/10.1016/j.carbon.2006.03.019
2.　Iijima, S. *Nature* **1991**, *354*, 56.
　　https://doi.org/10.1038/354056a0
3.　Oberlin, A.; Endo, M.; Koyama, T. *J. Cryst. Growth* **1976**, *32*, 335.
　　https://doi.org/10.1016/0022-0248(76)90115-9
4.　Dresselhaus, M. S.; Dresselhaus, G.; Avouris, P. *Carbon Nanotubes : Synthesis, Structure, Properties, and Applications*; Springer: Berlin; New York, 2001.
　　https://doi.org/10.1007/3-540-39947-X
5.　Wei, B. Q.; Vajtai, R.; Ajayan, P. M. *Appl. Phys. Lett.* **2001**, *79*, 1172.
　　https://doi.org/10.1063/1.1396632
6.　Baughman, R. H.; Zakhidov, A. A.; de Heer, W. A. *Science* **2002**, *297*, 787.
　　https://doi.org/10.1126/science.1060928
7.　Charlier, J. C.; Blase, X.; Roche, S. *Rev. Mod. Phys.* **2007**, *79*, 677.
　　https://doi.org/10.1103/RevModPhys.79.677
8.　Collins, P. G.; Bradley, K.; Ishigami, M.; Zettl, A. *Science* **2000**, *287*, 1801.
　　https://doi.org/10.1126/science.287.5459.1801
9.　Martin, C. R.; Kohli, P. *Nat. Rev. Drug Discov.* **2003**, *2*, 29.
　　https://doi.org/10.1038/nrd988
10.　Andrews, R.; Weisenberger, M. C. *Curr. Opin. Solid St. M.* **2004**, *8*, 31.
　　https://doi.org/10.1016/j.cossms.2003.10.006
11.　Vaisman, L.; Marom, G.; Wagner, H. D. *Adv. Funct. Mater.* **2006**, *16*, 357.
　　https://doi.org/10.1002/adfm.200500142
12.　Hirsch, A.; Vostrowsky, O. *Top. Curr. Chem.* **2005**, *245*, 193.
　　https://doi.org/10.1007/b98169
13.　Tasis, D.; Tagmatarchis, N.; Bianco, A.; Prato, M. *Chem. Rev.* **2006**, *106*, 1105.
　　https://doi.org/10.1021/cr050569o
14.　Liu, J.; Rinzler, A. G.; Dai, H.; Hafner, J. H.; Bradley, R. K.; Boul, P. J.; Lu, A.; Iverson, T.; Shelimov, K.; Huffman, C. B.; Rodriguez-Macias, F.; Shon, Y.-S.; Lee, T. R.; Colbert, D. T.; Smalley, R. E. *Science* **1998**, *280*, 1253.
　　https://doi.org/10.1126/science.280.5367.1253
15.　Chen, J.; Hamon, M. A.; Hu, H.; Chen, Y.; Rao, A. M.; Eklund, P. C.; Haddon, R. C. *Science* **1998**, *282*, 95.
　　https://doi.org/10.1126/science.282.5386.95
16.　Ziegler, K. J.; Gu, Z.; Peng, H.; Flor, E. L.; Hauge, R. H.; Smalley, R. E. *J. Am. Chem. Soc.* **2005**, *127*, 1541.
　　https://doi.org/10.1021/ja044537e
17.　Datsyuk, V.; Kalyva, M.; Papagelis, K.; Parthenios, J.; Tasis, D.; Siokou, A.; Kallitsis, I.; Galiotis, C. *Carbon* **2008**, *46*, 833.
　　https://doi.org/10.1016/j.carbon.2008.02.012
18.　Zhang, J.; Zou, H.; Qing, Q.; Yang, Y.; Li, Q.; Liu, Z.; Guo, X.; Du, Z. *J. Phys. Chem. B* **2003**, *107*, 3712.
　　https://doi.org/10.1021/jp027500u
19.　Spitalský, Z.; Krontiras, C. A.; Georga, S. N.; Galiotis, C. *Compos. Part A-Appl. S.* **2009**, *40*, 778.
20.　Hu, C.-C.; Su, J.-H.; Wen, T.-C. *J. Phys. Chem. Solids* **2007**, *68*, 2353.
　　https://doi.org/10.1016/j.jpcs.2007.07.002

21. Hu, H.; Zhao, B.; Itkis, M. E.; Haddon, R. C. *J. Phys. Chem. B* **2003**, *107*, 13838.
https://doi.org/10.1021/jp035719i

22. Rosca, I. D.; Watari, F.; Uo, M.; Akasaka, T. *Carbon* **2005**, *43*, 3124.
https://doi.org/10.1016/j.carbon.2005.06.019

23. Marshall, M. W.; Popa-Nita, S.; Shapter, J. G. *Carbon* **2006**, *44*, 1137.
https://doi.org/10.1016/j.carbon.2005.11.010

24. Kosynkin, D. V.; Higginbotham, A. L.; Sinitskii, A.; Lomeda, J. R.; Dimiev, A.; Price, B. K.; Tour, J. M. *Nature* **2009**, *458*, 872.
https://doi.org/10.1038/nature07872

25. Hiura, H.; Ebbesen, T. W.; Tanigaki, K. *Adv. Mater.* **1995**, *7*, 275.
https://doi.org/10.1002/adma.19950070304

26. Simmons, J. M.; Nichols, B. M.; Baker, S. E.; Marcus, M. S.; Castellini, O. M.; Lee, C. S.; Hamers, R. J.; Eriksson, M. A. *J. Phys. Chem. B* **2006**, *110*, 7113.
https://doi.org/10.1021/jp0548422

27. Bower, C.; Kleinhammes, A.; Wu, Y.; Zhou, O. *Chem. Phys. Lett.* **1998**, *288*, 481.
https://doi.org/10.1016/S0009-2614(98)00278-4

28. Martínez, M. T.; Callejas, M. A.; Benito, A. M.; Cochet, M.; Seeger, T.; Ansón, A.; Schreiber, J.; Gordon, C.; Marhic, C.; Chauvet, O.; Fierro, J. L. G.; Maser, W. K. *Carbon* **2003**, *41*, 2247.
https://doi.org/10.1016/S0008-6223(03)00250-1

29. Ren, F.; Kanaan, S. A.; Khalkhal, F.; Loebick, C. Z.; Haller, G. L.; Pfefferle, L. D. *Carbon* **2013**, *63*, 61.
https://doi.org/10.1016/j.carbon.2013.06.039

30. Zhang, H.; Guo, H.; Deng, X.; Gu, P.; Chen, Z.; Jiao, Z. *Nanotechnology* **2010**, *21*.

31. Cho, S.; Kikuchi, K.; Kawasaki, A. *Carbon* **2011**, *49*, 3865.
https://doi.org/10.1016/j.carbon.2011.05.023

32. Bergeret, C. l.; Cousseau, J.; Fernandez, V.; Mevellec, J.-Y.; Lefrant, S. *J. Phys. Chem. C* **2008**, *112*, 16411.
https://doi.org/10.1021/jp806602t

33. Wepasnick, K. A.; Smith, B. A.; Bitter, J. L.; Fairbrother, D. H. *Anal. Bioanal. Chem.* **2010**, *396*, 1003.
https://doi.org/10.1007/s00216-009-3332-5

34. Meier, M. S.; Andrews, R.; Jacques, D.; Cassity, K. B.; Qian, D. *J. Mater. Chem.* **2008**, *18*, 4143.
https://doi.org/10.1039/b809348b

35. Meier, M. S.; Selegue, J. P.; Cassity, K. B.; Kaur, A. P.; Qian, D. *J. Phys-Condens. Mat.* **2010**, *22*, 334219.

36. Qian, D.; Andrews, R.; Jacques, D.; Kichambare, P.; Lian, G.; Dickey, E. C. *J. Nanosci. Nanotech.* **2003**, *3*, 93.
https://doi.org/10.1166/jnn.2003.159

37. Andrews, R.; Jacques, D.; Qian, D.; Dickey, E. C. *Carbon* **2001**, *39*, 1681.
https://doi.org/10.1016/S0008-6223(00)00301-8

38. Bom, D.; Andrews, R.; Jacques, D.; Anthony, J.; Chen, B.; Meier, M. S.; Selegue, J. P. *Nano Lett.* **2002**, *2*, 615.
https://doi.org/10.1021/nl020297u

39. Wang, Y. H.; Shan, H. W.; Hauge, R. H.; Pasquali, M.; Smalley, R. E. *J. Phys. Chem. B* **2007**, *111*, 1249.
https://doi.org/10.1021/jp068229+

40. Dong, H.; Zhao, Y.; Tang, Y.; Burkert, S. C.; Star, A. *ACS Appl. Mater. Inter.* **2015**, *7*, 10734.
https://doi.org/10.1021/acsami.5b00447

41. Hummers, W. S.; Offeman, R. E. *J. Am. Chem. Soc.* **1958**, *80*, 1339.
https://doi.org/10.1021/ja01539a017

42. Lerf, A.; He, H.; Forster, M.; Klinowski, J. *J. Phys. Chem. B* **1998**, *102*, 4477.

https://doi.org/10.1021/jp9731821

43. Patrick, J. W. *Porosity in Carbons: Characterization and Applications*; Halsted Press: New York, 1995.

44. Guerard, D.; Herold, A. *Carbon* **1975**, *13*, 337.
    https://doi.org/10.1016/0008-6223(75)90040-8

45. Lin, K.; Xu, Y.; He, G.; Wang, X. *Mater. Chem. Phys.* **2006**, *2006*, 190.

46. Endo, M.; Kim, Y. A.; Hayashi, T.; Fukai, Y.; Oshida, K.; Terrones, M.; Yanagisawa, T.; Higaki, S.; Dresselhaus, M. S. *Appl. Phys. Lett.* **2002**, *80*, 1267.
    https://doi.org/10.1063/1.1450264

47. Yang, Y.; Rosalie, J.; Bourgeois, L.; Webley, P. A. *Mater. Res. Bull.*, *43*, 2368.
    https://doi.org/10.1016/j.materresbull.2007.08.020

48. Monthioux, M.; Noe, L.; Dussault, L.; Dupin, J. C.; Latorre, N.; Ubieto, T.; Romeo, E.; Royo, C.; Monzon, A.; Guimon, C. *J. Mater. Chem.* **2007**, *17*, 4611.
    https://doi.org/10.1039/b707742d

49. Cheng, H.-Y.; Zhu, Y.-A.; Sui, Z.-J.; Zhou, X.-G.; Chen, D. *Carbon* **2012**, *50*, 4359.
    https://doi.org/10.1016/j.carbon.2012.05.005

50. Vera-Agullo, J.; Varela-Rizo, H.; Conesa, J. A.; Almansa, C.; Merino, C.; Martin-Gullon, I. *Carbon* **2007**, *45*, 2751.
    https://doi.org/10.1016/j.carbon.2007.09.040

51. Xu, F. F.; Bando, Y.; Golberg, D. *New J. Phys.* **2003**, *5*, 118.
    https://doi.org/10.1088/1367-2630/5/1/118

52. Kim, Y.-A.; Hayashi, T.; Naokawa, S.; Yanagisawa, T.; Endo, M. *Carbon* **2005**, *43*, 3005.
    https://doi.org/10.1016/j.carbon.2005.06.037

53. Li, J.; Kaur, A. P.; Meier, M. S.; Cheng, Y.-T. *J. Appl. Electrochem.* **2014**, *44*, 179.
    https://doi.org/10.1007/s10800-013-0625-3

54. Thippani, T.; Mandal, S.; Wang, G.; Ramani, V. K.; Kothandaraman, R. *RSC Adv.* **2016**, *6*, 71122.
    https://doi.org/10.1039/C6RA13414A

55. Kim, K. H.; Brunel, D.; Gohier, A.; Sacco, L.; Châtelet, M.; Cojocaru, C. S. *Adv. Mater.* **2014**, *26*, 4363.
    https://doi.org/10.1002/adma.201400775

56. Fu, Y.; Romay, V.; Liu, Y.; Ibarlucea, B.; Baraban, L.; Khavrus, V.; Oswald, S.; Bachmatiuk, A.; Ibrahim, I.; Rümmeli, M.; Gemming, T.; Bezugly, V.; Cuniberti, G. *Sensor. Actuat. B-Chem.* **2017**, *249*, 691.